Role of the phosphoinositide phosphatase *FIG4* gene in familial epilepsy with polymicrogyria

Stéphanie Baulac, PhD
Guy M. Lenk, PhD*
Béatrice Dufresnois*
Bouchra Ouled Amar Bencheikh, PhD
Philippe Couarch
Julie Renard
Peter A. Larson
Cole J. Ferguson, MD, PhD
Eric Noé
Karine Poirier, PhD
Christine Hubans, PhD
Stéphanie Ferreira, PhD
Renzo Guerrini, MD
Reda Ouazzani, MD
Khalid Hamid El Hachimi, PhD
Miriam H. Meisler, PhD
Eric Leguern, MD, PhD

Correspondence to Prof. Leguern: eric.leguern@psl.aphp.fr

ABSTRACT

Objective: The aim of this study was to identify the causal gene in a consanguineous Moroccan family with temporo-occipital polymicrogyria, psychiatric manifestations, and epilepsy, previously mapped to the 6q16–q22 region.

Methods: We used exome sequencing and analyzed candidate variants in the 6q16–q22 locus, as well as a rescue assay in *Fig4*-null mouse fibroblasts and immunohistochemistry of *Fig4*-null mouse brains.

Results: A homozygous missense mutation (p.Asp783Val) in the phosphoinositide phosphatase gene *FIG4* was identified. Pathogenicity of the variant was supported by impaired rescue of the enlarged vacuoles in transfected fibroblasts from *Fig4*-deficient mice. Histologic examination of *Fig4*-null mouse brain revealed neurodevelopmental impairment in the hippocampus, cortex, and cerebellum as well as impaired cerebellar gyration/foliation reminiscent of human cortical malformations.

Conclusions: This study extends the spectrum of phenotypes associated with *FIG4* mutations to include cortical malformation associated with seizures and psychiatric manifestations, in addition to the previously described Charcot-Marie-Tooth disease type 4J and Yunis-Varón syndrome. ***Neurology*®** **2014;82:1068–1075**

GLOSSARY

cDNA = complementary DNA; **chr6** = chromosome 6; **CMT4J** = Charcot-Marie-Tooth disease type 4J; **GFP** = green fluorescent protein; ***plt*** = pale tremor; **WT** = wild-type; **YVS** = Yunis-Varón syndrome.

Polymicrogyria is a malformation of the cerebral cortex characterized by abnormal lamination and folding. As a result, the deeper cortical layers develop abnormally and an excessive number of small gyri form within the cortex.[1] Polymicrogyria belongs to the group of cortical malformations secondary to postmigrational development.[1] Clinical manifestations depend on the extent and location of the polymicrogyric cortex and range from asymptomatic to a severe phenotype variably including intractable epilepsy, cognitive impairment, and neurologic deficits.[1] Causes of polymicrogyria are heterogeneous and include acquired and genetic etiology. Several genes have been identified for autosomal recessive forms of polymicrogyria: *GPR56*[2] in bilateral frontoparietal polymicrogyria; *KBP*[3] in polymicrogyria with microcephaly; and the RAB GTPase genes including *RAB3GAP1*,[4] *RAB3GAP2*,[5] and *RAB18*[6] in Warburg Micro syndrome characterized by bilateral frontal polymicrogyria and thinning of the corpus callosum. Dominant mutations in *TUBA1A*,[7] *TUBB2B*,[8] and *TUBB3*[9] have been associated with frontoparietal or diffuse polymicrogyria, in *TUBA8*[10] with diffuse polymicrogyria with agenesis of corpus callosum and optic nerve hypoplasia, in *COL18A1*[11] with the Knobloch syndrome, and in *SRPX2*[12] with perisylvian polymicrogyria with rolandic seizures and speech dyspraxia.

We previously reported a consanguineous Moroccan family with segregation of an autosomal recessive phenotype associating polymicrogyria, epilepsy, and psychiatric manifestations with linkage

Supplemental data at Neurology.org

*These authors contributed equally to this work.

From INSERM (S.B., B.D., B.O.A.B., P.C., J.R., E.N., K.H.E.H., E.L.), U1127; Sorbonne Universités, UPMC Univ Paris 06 (S.B., B.D., B.O.A.B., P.C., J.R., E.N., K.H.E.H., E.L.), UM 75; CNRS (S.B., B.D., B.O.A.B., P.C., J.R., E.N., K.H.E.H., E.L.), UMR 7225, ICM, Paris, ICM, (S.B., B.D., B.O.A.B., P.C., J.R., E.N., K.H.E.H., E.L.) Paris, F-75013 Paris, France; Department of Human Genetics (G.M.L., P.A.L., C.J.F., M.H.M.), University of Michigan, Ann Arbor; Service de Neurophysiologie Clinique (B.O.A.B.), Hôpital des Spécialités, Centre Hospitalier Ibn Sina Rabat, Morocco; Genetics and Pathophysiology of Neurodevelopmental and Neuromuscular Diseases (K.P.), Cochin Institute, Paris; GenoScreen (C.H., S.F.), Lille, France; Neuroscience Department (R.G.), Children's Hospital A. Meyer, University of Florence and IRCCS Stella Maris, Pisa, Italy; Laboratoire de Neurogénétique (K.H.E.H.), Ecole Pratique des Hautes Etudes, Paris; and Département de Génétique et de Cytogénétique (E.L.), AP-HP Groupe hospitalier Pitié-Salpêtrière, Paris, France.

Go to Neurology.org for full disclosures. Funding information and disclosures deemed relevant by the authors, if any, are provided at the end of the article.

on chromosome 6q16–q22.[13] In this study, we performed whole-exome sequencing and identified a variant at the homozygous state in *FIG4*, a gene that was previously implicated in Charcot-Marie-Tooth disease type 4J (CMT4J)[14] and in Yunis-Varón syndrome (YVS).[15] The causality of this mutation was reinforced by a functional assay and the study of cortical development in *Fig4*-deficient mice.

METHODS Standard protocol approvals, registrations, and patient consents. Nine family members (3 affected and 6 unaffected) gave written consent to participate in the study in accordance with the local committee of the University Mohammed V-Souissi, Rabat, Morocco (no. 108).

Whole-exome sequencing. Exons from 3 μg of genomic DNA of patient V.11 were captured using the SureSelect kit following the manufacturer's protocols (Agilent, Santa Clara, CA). The whole-exome DNA library was sequenced on the HiSeq2000 Illumina Genome Analyzer (Illumina, San Diego, CA). Sequence reads were mapped to the reference human genome using whole genomic sequence, refgene.txt file, and reflink.txt (UCSC hg19) using the BWA v0.5.9 algorithm (http://samtools.sourceforge.net). A mean depth of 40× covered the candidate homozygosity region on chromosome 6 (chr6: 103015795–117950828) for all exons. Only one gene of the region, *LOC285758* (114189178–114194512), was not covered, and was probably absent from the design in the SureSelect protocol. Variant detection was performed with the SAMTools v0.1.17 software (http://samtools.sourceforge.net) and filtered by different scripts (Perl) to fit quality threshold: depth ≥10× and a percentage of reads between 40% and 60%. Variants were annotated according to snp132.txt.

Validation of exome variants and screening of a patient cohort by Sanger sequencing. Analysis of exome sequencing focused on the 6q16–q22 locus (chr6: 103,015,795–117,950,828; hg19), the unique region with positive logarithm of odds scores. Variants found by exome sequencing were validated, and segregation analysis was performed by Sanger sequencing using the Big-Dye Terminator kit on an ABI Prism 3730 DNA Analyzer (Applied Biosystems, Foster City, CA). Mutation interpretation was assessed with Alamut software (Interactive Biosoftware, Rouen, France). The effect of amino acid substitution on protein function was predicted using SIFT, PolyPhen-2, and MutationTaster. All 23 exons and intron-exon junctions of *FIG4* (RefSeqNM_014845.5) were sequenced in 33 additional unrelated patients with polymicrogyria.

Phenotype rescue assay. The p.Asp783Val mutation was incorporated into the mouse *Fig4* complementary DNA (cDNA) clone by site-directed mutagenesis and the construct was completely sequenced. Mouse fibroblasts were isolated from P0 mouse tail biopsy by digestion with collagenase type 2 (Worthington Biochemical, Lakewood, NJ) and cultured in RPMI 1640 supplemented with 15% fetal bovine serum and containing penicillin, streptomycin, and amphotericin. Experiments were performed at passage 3 to 5.[16] Fibroblasts at 50% confluence were cotransfected with *Fig4* cDNA and green fluorescent protein (GFP) cDNA. GFP-positive cells were imaged 18 hours after transfection with an inverted Leica DM IRB microscope (Leica Microsystems, Buffalo Grove, IL) equipped with epifluorescence and an Olympus DP30 BW digital camera (Olympus, Center Valley, PA). Rescued cells were defined as GFP-positive cells with fewer than 6 vacuoles. The cell area occupied by vacuoles was quantitated using ImageJ software.

Caspase 3/7 activity assay. Ten percent brain homogenates were prepared, and cleavage of aminoluciferin-tagged DEVD peptide was measured. After centrifugation of homogenates at 15,000*g*, protein concentration in the supernatant was adjusted to 0.02 mg/mL. An equal volume of homogenate and Caspase-Glo 3/7 reagent (Promega, Madison, WI) was added to a white-walled 96-well plate and incubated at room temperature for 60 minutes. Luminescence was read on a Promega GloMax-Multiplate luminometer.

Western blot. Whole mouse brains were removed and lysed in 5 M urea, 2.5% sodium dodecyl sulfate, 50 mM Tris, 30 mM NaCl buffer. Protein concentration was determined by the Bradford method. Twenty-five micrograms of each sample was separated on 10% Tris-glycine polyacrylamide gels and analyzed by Western blot using monoclonal anti-FIG4 antibody (NeuroMab clone N202/7) and rabbit polyclonal anti-actin antibody (Sigma-Aldrich, St. Louis, MO).

Histochemistry. Brains from mice aged P0 and P4 (n = 5 for each genotype) were removed and postfixed for 24 hours in 4% paraformaldehyde in 0.1 mol/L phosphate buffer, pH 7.4. Seven-micrometer-thick paraffin sections were cut. Immunohistochemistry was performed using rabbit Calbindin D-28k (Swant, Marly, Switzerland) and Nissl counterstaining using standard procedures.

Morphometry. A drawing of the cerebellar fissures of midsagittal sections at 40× was made as previously reported[17] using a Leica SCN slide scanner. We measured 6 principal fissures (precentral, preculminate, primary, prepyramidal, secondary, and posterolateral) by the Image Processing Toolbox of CaloPix software viewer (http://www.teleslide.fr). Measurements of fissures are given as mean (± standard error) and compared using a Mann-Whitney test.

RESULTS Clinical characterization. Clinical data of the Moroccan kindred with 6 affected siblings were previously reported.[13] Since our previous publication, V.8 died of a seizure and V.9 committed suicide. In this family, 6 patients had epilepsy (complex focal and secondarily generalized seizures). Seizures consisted of visual hallucinations, sometimes followed by auditory hallucinations, as well as epigastric and thoracic oppression or neurovegetative symptoms suggesting that the epileptic discharges spread to the temporal lobe. The course and severity of epilepsy were variable from one patient to another for age at onset, ranging from birth (V.5 and V.11) to 24 years (V.1), and frequency of seizures ranging from 1 to 2 per month (V.1) to several per day (V.8 and V.9). The outcome of epilepsy largely depended on the compliance of patients with their antiepileptic medication; sudden death (SUDEP) occurred in 2 patients, V.5 and V.6, who were untreated. In addition, severe psychiatric manifestations were reported in 4 patients (V.1, V.8, V.9, and V.11). A psychotic disorder with aggressiveness and delirium was diagnosed in patients V.8 and V.11. Patient V.1 manifested chronic aggressiveness toward relatives. In addition, 2 patients (V.1, V.9) committed suicide.

The 3 patients examined by brain MRI, V.8, V.9, and V.11, exhibited a thickened irregular cortex in the lateral occipital lobes with small gyri and were diagnosed with bilateral occipital polymicrogyria.[13] Upon critical

re-evaluation of MRI in these 3 patients by the neurologist participating in this study (R.G.), we concluded that the cortical abnormality also involved the lateral part of the posterior temporal lobes. Patients therefore had temporo-occipital rather than occipital polymicrogyria (figure 1). Family members IV.1 (the father) and V.7 (a nonaffected sibling) had normal brain MRI.

Molecular studies. We previously mapped the causative gene to a unique 14-Mb locus on chromosome 6q16–q22.[13] Here, we performed whole-exome sequencing in one patient (V.11),[13] and focused our analysis on the 6q16–q22 region (chr6: 103,015,795–117,950,828; hg19). This rare phenotype segregated as an autosomal recessive disorder in the consanguineous pedigree. Therefore, we filtered nonsynonymous and insertion/deletion variants located in this interval in the homozygous state with frequency <1% in the databases (dbSNP135, 1000 Genomes Project database, and National Heart, Lung, and Blood Institute exome variant server database). Only 2 missense variants were identified: c.716T>G/p.Leu239Arg in *TUBE1* that was previously excluded because of its high frequency in a Maghrebian cohort of controls (2% allele frequency)[13] and c.2348A>T/p.Asp783Val located in exon 20 of the *FIG4* gene. Both parents were heterozygous for the variant in *FIG4*, which fully cosegregated with the phenotype in the family (figure 2A). This variant was absent from the dbSNP135, 1000 Genomes Project, and exome variant server databases. Additionally, it was not found in 750 in-house controls, including 422 ethnically matched from Maghreb. At the protein level, the Asp783 residue is located in the C-terminus of the protein (figure 2B) and is invariant in mammals and terrestrial vertebrates (figure 2C). Asp and Val have a high Grantham distance of 152 (0–215) reflecting the chemical dissimilarity between the negatively charged, polar aspartate residue and the hydrophobic valine residue. The prediction software tools MutationTaster, PolyPhen-2, and SIFT predicted that this variant was pathogenic, possibly damaging, and tolerated, respectively. Sanger sequencing of the complete coding region of *FIG4* did not reveal pathogenic mutations in 33 additional patients with various types of polymicrogyria.

Figure 1 Brain MRI

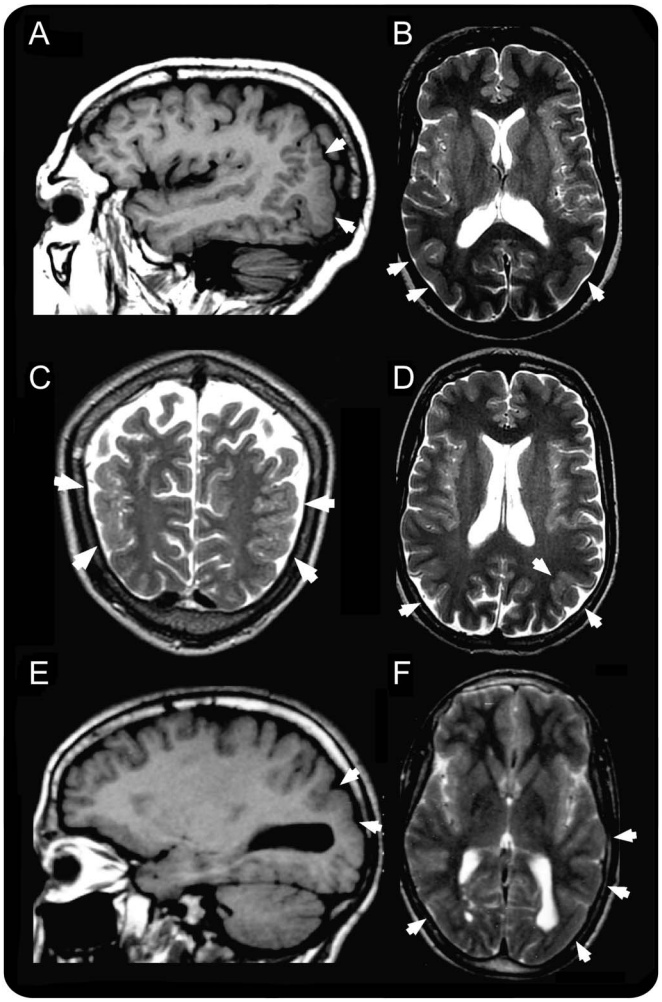

(A, B) Patient V.8, (C, D) patient V.9, and (E, F) patient V.11. Images A and E are T1-weighted sagittal sections; B, D, and F are T2-weighted axial sections; and C is a T2-weighted coronal section. The areas of abnormal cortical development in the temporo-occipital areas are indicated by the white arrows and are consistent in all 3 patients with a combination of increased cortical thickness, smooth cortex, overfolding, and microgyri.

Functional studies in *Fig4*-null fibroblasts. *FIG4* encodes a phosphoinositide 5-phosphatase that regulates the cellular abundance of the signaling lipid PI(3,5)P2, and thus endosomal trafficking and autophagy. Complete loss of *Fig4* in the null mouse mutant pale tremor (*plt*) results in extensive neurodegeneration of the central and peripheral nervous system.[14,18] The cytoplasm of cultured fibroblasts from *plt* mice is filled with enlarged vacuoles.[14,18] To assess the functional effect of the p.Asp783Val (D783V) variant, we performed a phenotype rescue of vacuolization in cultured cells. Transfection of *Fig4*-null cells with wild-type (WT) *Fig4* cDNA rescues the vacuoles, while the Fig4-D783V is defective in rescue (figure 2D). In the combined data from 3 independent experiments represented in figure 2E, the WT cDNA completely corrected vacuolization in 60% of transfected cells (334/558) while the D783V cDNA corrected vacuolization in only 33% of transfected cells (262/797) ($p < 0.01$, t test). In cells that were not completely corrected by the mutant cDNA, the total area occupied by vacuoles was significantly reduced by expression of the D783V cDNA ($p < 0.001$, Yates correction χ^2) (figure 2F). These data demonstrate that the D783V mutation causes partial but not complete loss of FIG4 function.

Histologic studies in *Fig4*-null brains. To further investigate the role of *Fig4* in cortical development, we examined

Figure 2 **Identification of *FIG4* mutation**

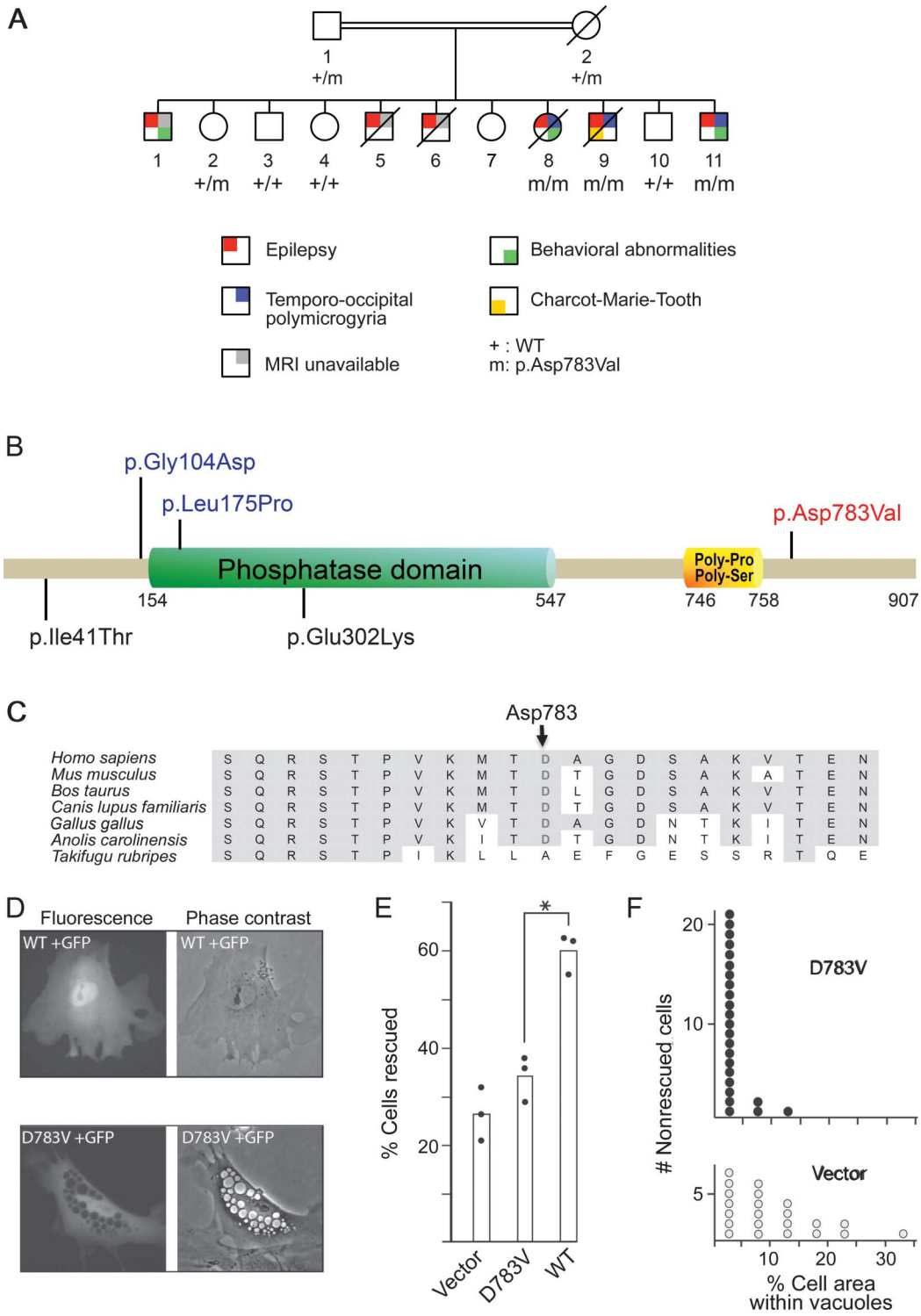

(A) Pedigree of the family with segregation of the *FIG4* variant. Only generations IV and V are shown.[13] (B) FIG4 is a multidomain protein with a protein interaction domain at the N-terminus, a SAC phosphatase domain in the central region, and poly-Pro and poly-Ser domains within the C-terminal. The mutation identified in this study is indicated in red, and missense mutations previously reported in Charcot-Marie-Tooth disease type 4J[21] and Yunis-Varón syndrome[15] are indicated in black and blue, respectively. (C) Multiple protein alignment showing conservation of the aspartate (D) residue in position 783 in orthologs of FIG4 across species. (D) Phenotype rescue in *Fig4*-null fibroblasts of *plt* mice. Mutant or wild-type (WT) *Fig4* cDNA was cotransfected with GFP into *Fig4*-null fibroblasts. The large intracytoplasmic vesicles characteristic of *Fig4*-null fibroblasts were rescued in 60% of cells by the WT cDNA (top panels) but in only 33% of cells by the D783V mutant cDNA (bottom panels). (E) Percent of transfected (GFP-positive) fibroblasts that lack vacuoles. The results of 3 independent experiments are indicated. *$p < 0.01$. (F) The D783V mutant retains partial activity. In nonrescued cells from panel E, the percentage of cell area covered by vacuoles in cells expressing D783V (3.3% ± 0.6%, n = 24) is smaller than that in cells receiving vector only (10.3% ± 1.8%, n = 22) (2-tailed *p* value <0.001). Transfection of the mutant cDNA does not completely rescue the formation of vacuoles but does reduce the severity of vacuolization. cDNA = complementary DNA; GFP = green fluorescent protein; *plt* = pale tremor.

the temporal expression of the protein in developing mouse brain by Western blot of whole-brain lysates between embryonic day 10.5 (E10.5) and postnatal day P14, before spongiform degeneration. FIG4 protein expression could be detected as early as E10.5, consistent with a neurodevelopmental role (figure e-1 on the *Neurology*® Web site at Neurology.org). We then asked whether neurodevelopmental defects of the brain were present in *plt* mice, as in patients with polymicrogyria. No obvious macroscopic modification was observed in brains of *plt* mice at postnatal age P0 and P4 (data not shown). However, histologic Nissl staining revealed increased neuronal density in *plt* mice in all cortical layers at P0 (figures 3A and e-2), which was no longer present at P4 (figure 3A), likely due to cell death. Indeed, during this time interval, the level of the apoptosis-associated activated caspase 3/7 was transiently elevated in the mutant brain (figure 3B). Because expression of calbindin D-28k is correlated with postnatal maturation of hippocampal dentate granule cells[19] and dendritic arborization,[20] we performed anti-calbindin immunohistochemistry of the WT and *plt* brains (n = 5 for each). Calbindin staining was drastically decreased in *plt* mice, indicating delayed maturation of interneurons and dentate granule cells and their processes in the hippocampus at P4 (figure 3C), in the soma and dendritic tree of Purkinje cells at P0 (figure e-3A) and P4 (figure 3D), and in cortical interneurons of *plt* mice (figure e-3B). Morphometric study of postnatal cerebellar development at P4 revealed a significant reduction in the depth of all fissures in *plt* mice, with the exception of the primary fissure, demonstrating delayed cerebellar gyration/foliation (Mann-Whitney test, $p < 0.05$) (figures 3E and e-4). These findings support both impaired molecular development (decreased calbindin expression) and impaired anatomical development (gyration) in *Fig4*-deficient mice, reflecting postmigration abnormalities that are considered to be the major mechanisms underlying polymicrogyria in human.[1]

DISCUSSION The present study extends to polymicrogyria the spectrum of phenotypes associated with *FIG4* mutations, which were previously identified in CMT4J[14,21] and YVS[15] (figure 2B). A key question is how *FIG4* mutations can lead to such diverse autosomal recessive disorders: (1) CMT4J, a peripheral neuropathy, (2) YVS, in which neurodegeneration and brain malformations are associated with cleidocranial dysplasia, digital anomalies, and early death, and (3) temporo-occipital polymicrogyria with seizures and psychiatric features. The major distinction is that patients with YVS are homozygous or compound heterozygous for null mutations of *FIG4*, and thus exhibit complete loss of function, similar to the *plt* mouse. In contrast, patients with CMT4J and polymicrogyria retain partial function of FIG4. Consistent with this view, the missense mutations found in patients with YVS (figure 2B) exhibit complete loss of function in the rescue of vacuolization by *Fig4*-null fibroblasts,[15] while partial function is demonstrated for the missense mutations p.Ile41Thr[16] and p.Asp783Val (this study). Spongiform neurodegeneration is only seen with complete loss of FIG4 function in the *plt* mouse and patients with YVS. Patients with CMT4J are compound heterozygotes carrying a null allele in combination with the partial loss-of-function allele p.Ile41Thr mutation[14,21] (figure 2B). The p.Ile41Thr mutation impairs protein stability and interaction with the scaffold protein VAC14, but overexpression of the mutant protein can rescue lethality of the *plt* mouse, demonstrating residual function.[16] Based on their location in different protein domains, the p.Asp783Val mutation causing polymicrogyria might impair interaction with a different set of proteins than p.Ile41Thr, thereby resulting in cortical malformation rather than peripheral neuropathy. There is some phenotypic overlap between the disorders caused by *FIG4* mutations, because patients with YVS exhibit brain malformations including underdeveloped gyri and polymicrogyria that are the hallmark of the phenotype associated with the p.Asp783Val mutation.[22,23] Interestingly, Walch et al.[22] noted that in one patient with YVS, the areas of neuronal vacuolization did not overlap with areas exhibiting pachygyria and polymicrogyria, indicating that the process of neurodegeneration might mask preceding cortical abnormalities. Two features present in the family we are describing could also modulate conclusions on phenotype-genotype correlations: (1) we noted enlarged cerebral ventricles at MRI in patients V.8, V.9, and V.11,[13] a feature also seen in *Fig4*-null mice,[14] which might reflect a neurodegenerative process much milder than that occurring in YVS; and (2) an axonal sensory and motor neuropathy was diagnosed in patient V.9 that is related to the peripheral neuropathy occurring in CMT4J.[13] However, in patients with CMT4J, the pathologic process is also demyelinating and associated with an age at onset that is variable, sometimes occurring in childhood. Because other patients of the family did not exhibit signs of neuropathy at age 23 (V.11), 35 (V.8), or 55 (V.1) years, it is uncertain whether the neuropathy diagnosed in patient V.9 is related to the *FIG4* mutation. In addition, the electrophysiologic examination of V.8 was fully normal.

Polymicrogyria is a common cortical malformation and is associated with different morphologic patterns and syndromes. Its pathogenesis is not fully understood; brain pathology demonstrates abnormal

Figure 3 Neurodevelopmental anomalies in *plt* mice

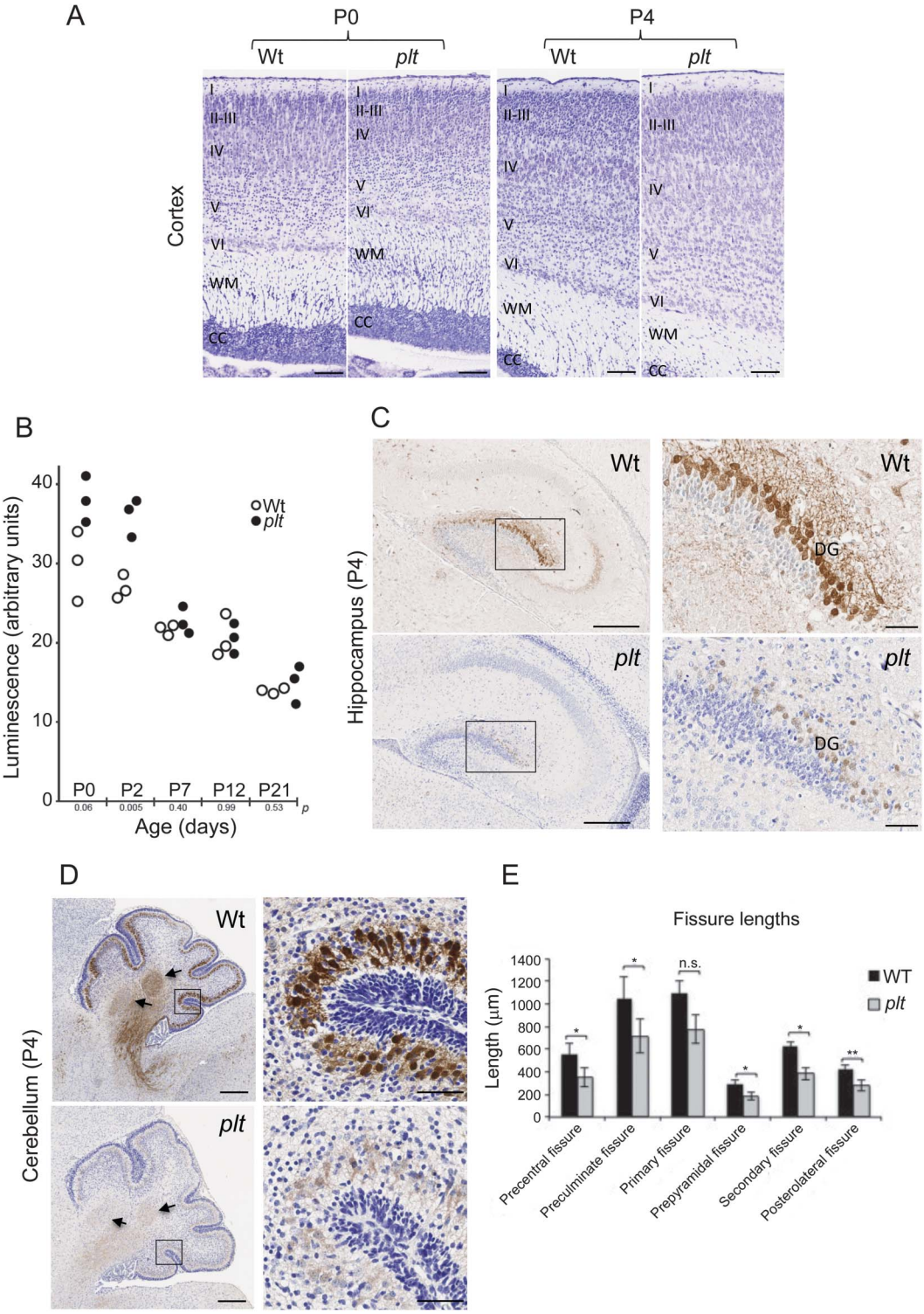

(A) Nissl staining of cortex from *plt* homozygote and WT littermate at postnatal days P0 and P4. Note presence of swollen neurons in layers IV and V of *plt* aged P4. Cortical layers are indicated as follows: I–VI, WM (white matter), CC (corpus callosum). (B) Caspase 3/7 activity was measured in brain homogenates from 3 animals of each genotype at the indicated postnatal age. An unpaired Student *t* test was used to generate *p* values at each age. (C) Weak calbindin immunoreactivity in hippocampus of *plt* mouse compared with WT littermates. Higher magnification of dorsal DG (boxed regions) shows many granule cells with a well-developed dendrite tree in the WT brain, while in the *plt*, there is weak staining of the perikaryon and no immunostaining of dendrite trees. (D) Very weak calbindin immunoreactivity in cerebellar cortex and deep nucleus (arrows) in *plt* mouse compared with WT littermate at P4. Boxed areas are focused on posterolateral fissures. Scale bars: A, 100 μm; C, 300 μm (boxed area 50 μm); D, 250 μm (boxed area 50 μm). (E) Histogram representing the fissure lengths in the cerebellum at P4 (n = 5). Significant differences between lengths of fissures were observed between WT and *plt*. *$p < 0.05$; **$p < 0.01$. DG = dentate gyrus; n.s. = not significant; *plt* = pale tremor; WT = wild-type.

development or loss of neurons in middle and deep cortical layers, variably associated with an unlayered cortical structure.[24] Clinical, pathologic, and imaging heterogeneity suggest that polymicrogyria is not a single malformation. Different types of single gene inheritance have been reported, and causative mutations have been identified in several genes such as *GPR56*,[2] *KBP*,[3] *NHEJ1*,[25] *TUBB2B*,[8] *TUBB3*,[9] *TUBA8*,[10] and *TUBA1A*[7] as well as *RAB3GAP1*,[4] *RAB3GA2*,[5] and *RAB18*[6] encoding Ras-related small GTPases that regulate membrane trafficking in organelles and transport of endolysosomal vesicles. The function of FIG4 is related to the Ras GTPases because it is involved in the control of intracellular PI(3,5)P2 concentration. The coordinated regulation of specific RABs and phosphoinositides is emerging as an important mechanism to ensure precision and fidelity of membrane trafficking,[26] which seems to be crucial for postmigrational development of neurons.

Our findings implicate *FIG4* in the pathogenesis of a temporo-occipital polymicrogyria associated with epilepsy and psychiatric manifestations. It is hoped that this discovery will shed light on the complex biology underlying the formation of cortical gyri and the role of PI(3,5)P2 signaling in this process.

AUTHOR CONTRIBUTIONS

S.B., B.O.A.B., P.C., J.R., E.N., K.P., C.H., S.F. collected and analyzed genetic data. G.M.L., P.A.L., C.J.F collected and analyzed data on functional studies. B.D., K.H.E.H. collected and analyzed neuropathologic data. R.G. analyzed neuroimaging and participated in the writing of the manuscript. R.O. collected and analyzed clinical data. S.B., M.H.M, E.L. supervised the work and wrote the manuscript.

ACKNOWLEDGMENT

The authors thank Murat Gunel and Jamel Chelly for providing DNAs of patients with cortical malformations; Fiona Francis and Mihaela Vlaicu for helpful discussion; Ashley Miller and Margaret Wu for assistance with quantitation of the vacuole area in cultured cells; and Frédéric Texier and Hélène Blanquart for exome sequencing and the ICM cell imaging platform and ICM histology platform.

STUDY FUNDING

S. Baulac received research support from Carnot Institute (CT010) and from the program Investissements d'avenir ANR-10-IAIHU-06. G.M. Lenk received research support from NIH R01 GM24872 and NIH U01 TR000433. B.O.A. Bencheikh received research support from the University Mohammed V-Souissi of Rabat in Morocco. K. Poirier received support from the Agence National de Recherche (ANR Blanc 1103 01, project R11039KK; ANR E-Rare-012-01, project E10107KP).

DISCLOSURE

S.B., G.M.L., B.D., B.O.A.B., P.C., J.R., C.J.F., E.N., K.P., R.O., K.H.E.H., M.H.M., and E.L. report no disclosures. P. Larson received research support from NIH R01 GM24872. C. Hubans and S. Ferreira are employees of GenoScreen company. R. Guerrini received honoraria from Biocodex, UCB, Eisai Inc., ValueBox, and ViroPharma, and research support from the Italian Ministry of Health, the European Community Sixth and Seventh Framework Thematic Priority Health, the Italian Ministry of Education, University and Research, the Tuscany Region, the Telethon Foundation, and the Mariani Foundation. R. Ouazzani received research support from the Programme d'Action Intégrée MA/108/04 between Morocco and France. K.H. El Hachimi reports no disclosures relevant to the manuscript. M. Meisler received research support from NIH R01 GM24872. E. Leguern received research support from Carnot Institute (CT010) and from the program Investissements d'avenir ANR-10-IAIHU-06. Go to Neurology.org for full disclosures.

Received July 10, 2013. Accepted in final form December 12, 2013.

REFERENCES

1. Barkovich AJ, Guerrini R, Kuzniecky RI, Jackson GD, Dobyns WB. A developmental and genetic classification for malformations of cortical development: update 2012. Brain 2012;135:1348–1369.
2. Piao X, Hill RS, Bodell A, et al. G protein-coupled receptor-dependent development of human frontal cortex. Science 2004;303:2033–2036.
3. Valence S, Poirier K, Lebrun N, et al. Homozygous truncating mutation of the KBP gene, encoding a KIF1B-binding protein, in a familial case of fetal polymicrogyria. Neurogenetics 2013;14:215–224.
4. Morris-Rosendahl DJ, Segel R, Born AP, et al. New RAB3-GAP1 mutations in patients with Warburg Micro syndrome from different ethnic backgrounds and a possible founder effect in the Danish. Eur J Hum Genet 2010;18:1100–1106.
5. Borck G, Wunram H, Steiert A, et al. A homozygous RAB3GAP2 mutation causes Warburg Micro syndrome. Hum Genet 2011;129:45–50.
6. Bem D, Yoshimura S, Nunes-Bastos R, et al. Loss-of-function mutations in RAB18 cause Warburg Micro syndrome. Am J Hum Genet 2011;88:499–507.
7. Poirier K, Keays DA, Francis F, et al. Large spectrum of lissencephaly and pachygyria phenotypes resulting from de novo missense mutations in tubulin alpha 1A (TUBA1A). Hum Mutat 2007;28:1055–1064.
8. Jaglin XH, Poirier K, Saillour Y, et al. Mutations in the beta-tubulin gene TUBB2B result in asymmetrical polymicrogyria. Nat Genet 2009;41:746–752.
9. Poirier K, Saillour Y, Bahi-Buisson N, et al. Mutations in the neuronal ss-tubulin subunit TUBB3 result in malformation of cortical development and neuronal migration defects. Hum Mol Genet 2010;19:4462–4473.
10. Abdollahi MR, Morrison E, Sirey T, et al. Mutation of the variant alpha-tubulin TUBA8 results in polymicrogyria with optic nerve hypoplasia. Am J Hum Genet 2009;85:737–744.
11. Sertie AL, Sossi V, Camargo AA, Zatz M, Brahe C, Passos-Bueno MR. Collagen XVIII, containing an endogenous inhibitor of angiogenesis and tumor growth, plays a critical role in the maintenance of retinal structure and in neural tube closure (Knobloch syndrome). Hum Mol Genet 2000;9:2051–2058.
12. Roll P, Rudolf G, Pereira S, et al. SRPX2 mutations in disorders of language cortex and cognition. Hum Mol Genet 2006;15:1195–1207.
13. Ben Cheikh BO, Baulac S, Lahjouji F, et al. A locus for bilateral occipital polymicrogyria maps to chromosome 6q16-q22. Neurogenetics 2009;10:35–42.
14. Chow CY, Zhang Y, Dowling JJ, et al. Mutation of FIG4 causes neurodegeneration in the pale tremor mouse and patients with CMT4J. Nature 2007;448:68–72.
15. Campeau PM, Lenk GM, Lu JT, et al. Yunis-Varon syndrome is caused by mutations in FIG4, encoding a phosphoinositide phosphatase. Am J Hum Genet 2013;92:781–791.
16. Lenk GM, Ferguson CJ, Chow CY, et al. Pathogenic mechanism of the FIG4 mutation responsible for Charcot-Marie-Tooth disease CMT4J. PLoS Genet 2011;7:e1002104.

17. Wahlsten D, Andison M. Patterns of cerebellar foliation in recombinant inbred mice. Brain Res 1991;557:184–189.
18. Ferguson CJ, Lenk GM, Jones JM, et al. Neuronal expression of Fig4 is both necessary and sufficient to prevent spongiform neurodegeneration. Hum Mol Genet 2012;21:3525–3534.
19. Abraham H, Orsi G, Seress L. Ontogeny of cocaine- and amphetamine-regulated transcript (CART) peptide and calbindin immunoreactivity in granule cells of the dentate gyrus in the rat. Int J Dev Neurosci 2007;25:265–274.
20. Rami A, Brehier A, Thomasset M, Rabie A. Cholecalcin (28-kDa calcium-binding protein) in the rat hippocampus: development in normal animals and in altered thyroid states—an immunocytochemical study. Dev Biol 1987;124:228–238.
21. Nicholson G, Lenk GM, Reddel SW, et al. Distinctive genetic and clinical features of CMT4J: a severe neuropathy caused by mutations in the PI(3,5)P(2) phosphatase FIG4. Brain 2011;134:1959–1971.
22. Walch E, Schmidt M, Brenner RE, et al. Yunis-Varon syndrome: evidence for a lysosomal storage disease. Am J Med Genet 2000;95:157–160.
23. Kulkarni ML, Vani HN, Nagendra K, et al. Yunis Varon syndrome. Indian J Pediatr 2006;73:353–355.
24. Guerrini R, Dobyns WB, Barkovich AJ. Abnormal development of the human cerebral cortex: genetics, functional consequences and treatment options. Trends Neurosci 2008;31:154–162.
25. Cantagrel V, Lossi AM, Lisgo S, et al. Truncation of NHEJ1 in a patient with polymicrogyria. Hum Mutat 2007;28:356–364.
26. Jean S, Kiger AA. Coordination between RAB GTPase and phosphoinositide regulation and functions. Nat Rev Mol Cell Biol 2012;13:463–470.